

See discussions, stats, and author profiles for this publication at: <https://www.researchgate.net/publication/231653641>

# Enhanced Optical Properties of Core/Shell/Shell CdTe/CdS/ZnO Quantum Dots Prepared in Aqueous Solution

ARTICLE in THE JOURNAL OF PHYSICAL CHEMISTRY C · NOVEMBER 2009

Impact Factor: 4.77 · DOI: 10.1021/jp905695f

---

CITATIONS

41

READS

152

## 8 AUTHORS, INCLUDING:



Fadi Aldeek

Florida Department of Agriculture and Con...

24 PUBLICATIONS 303 CITATIONS

[SEE PROFILE](#)



Lavinia Balan

French National Centre for Scientific Resea...

134 PUBLICATIONS 1,213 CITATIONS

[SEE PROFILE](#)



Jean-Pierre Malval

Université de Haute-Alsace

74 PUBLICATIONS 632 CITATIONS

[SEE PROFILE](#)



Raphaël Schneider

University of Lorraine

202 PUBLICATIONS 2,616 CITATIONS

[SEE PROFILE](#)

# Enhanced Optical Properties of Core/Shell/Shell CdTe/CdS/ZnO Quantum Dots Prepared in Aqueous Solution

Fadi Aldeek,<sup>†,‡</sup> Lavinia Balan,<sup>§</sup> Ghouti Medjahdi,<sup>||</sup> Thibault Roques-Carmes,<sup>‡</sup> Jean-Pierre Malval,<sup>§</sup> Christian Mustin,<sup>⊥</sup> Jaafar Ghanbaja,<sup>#</sup> and Raphaël Schneider<sup>\*,‡</sup>

LCPME, Nancy-University, CNRS, 405 rue de Vandoeuvre, 54506 Villers-lès-Nancy, France, DCPR, Nancy-University, CNRS, 1 rue Grandville, 54001 Nancy Cedex, France, DPG, UMR CNRS 7525, Université de Haute Alsace, 3 rue Alfred Werner, 68093 Mulhouse, France, IJL, Nancy-University, BP 70239, 54506 Vandoeuvre-lès-Nancy Cedex, France, LIMOS, Nancy-University, CNRS, BP 70239, 54506 Vandoeuvre-lès-Nancy Cedex, France, and SCMEM, Nancy-University, BP 70239, 54506 Vandoeuvre-lès-Nancy Cedex, France

Received: June 17, 2009; Revised Manuscript Received: September 22, 2009

New quantum dots (QDs) were fabricated with a core/shell/shell structure consisting of CdTe core/CdS shell/ZnO shell. Despite the high lattice mismatch between CdS and ZnO, a ZnO shell was successfully introduced by basic hydrolysis of Zn(OAc)<sub>2</sub> at the surface of core/shell CdTe/CdS QDs stabilized by 3-mercaptopropionic acid (MPA). The core/shell/shell CdTe/CdS/ZnO@MPA QDs exhibited a significant redshift of emission peaks (up to 50 nm for green-emitting CdTe/CdS QDs) when the shell grew. By changing the size of the core or the thickness of the ZnO shell, the emission colors of the obtained nanocrystals can be tuned between the green and red regions of the spectrum following an identical procedure. The influence of ZnO shell growth on photoluminescence (PL) quantum yields was found to be more pronounced for CdTe/CdS samples with green or yellow emission for which quantum yields increased up to three times. The epitaxial growth of the ZnO shell was confirmed by X-ray photoelectron spectroscopy and luminescence decay experiments. Because of the passivation of surface defects, a PL lifetime of 33.6 ns was measured for core/shell/shell CdTe/CdS/ZnO QDs prepared with a Zn/Cd ratio of 0.8, while it was only 17.7 ns for core/shell CdTe/CdS QDs.

## 1. Introduction

In the past decade, colloidal luminescent semiconductor nanocrystals, often referred to quantum dots (QDs), have attracted much attention because of their unique optical properties that are superior to those of conventional organic fluorophores. Indeed, their wide absorption spectrum, narrow emission, large extinction coefficients, and photostability are some of the most attractive characteristics.<sup>1–5</sup> Because of these properties, QDs are becoming a new class of powerful tools in biological and medical applications for sensing, labeling, optical imaging, cell separation, and treatment of disease.<sup>6–9</sup> However, these applications require QDs that are well-dispersed and stable in aqueous solution, thus creating a need to further engineer QD coatings because high-quality QDs are generally prepared via the organometallic route (e.g., core/shell CdSe/ZnS, core/shell/shell CdSe/CdS/ZnS, and core/shell/shell CdSe/CdTe/ZnSe) and are stabilized by hydrophobic ligands such as tri-*n*-octylphosphine/tri-*n*-octylphosphine oxide.<sup>10–12</sup> Several strategies (use of hydrophilic thiol stabilizer, incorporation into polymers or micelles, etc) have been developed to transfer hydrophobic QDs to the aqueous phase. Although these methods are efficient, they require additional steps. Moreover, the photoluminescence quantum yield (PL QY) of the QDs generally decreases when

they are transferred into water because of the high polarity of this solvent that breaks various equilibria related to the QDs.<sup>13</sup> Nevertheless, aqueous synthesis is an alternative strategy to directly prepare water-dispersed QDs. In addition, this method is cheaper, simpler, and less toxic. In recent years, methods of preparing luminescent QDs have been significantly improved. Nanocrystals such as CdSe<sup>14–17</sup> or CdTe<sup>17–19</sup> capped with small thioalkyl acids, generally thioglycolic acid (TGA) or 3-mercaptopropionic acid (MPA), have been prepared either by heating at 100 °C, the hydrothermal method, or microwave-assisted synthesis.<sup>20,21</sup> Modest QYs (generally lower than 20%) and poor biocompatibility of these QDs have however held back the potential applications of QDs prepared via an aqueous method.

The surface control of nanocrystals is a critical issue for enhancing photostability and luminescence efficiency.<sup>22</sup> In recent years, much effort has been invested in surface coating to enhance the chemical and optical stability of QDs. Because II–VI semiconductors have anionic and cationic surface sites, a classical organic capping leaves a relatively large number of unpassivated sites, and consequently, their PL QYs are generally modest. Moreover, the surface coverage of these QDs is limited because of the steric bulk of the capping ligand.<sup>17</sup> Heteroepitaxially growing an inorganic shell of a wider band gap semiconductor around the core improves the PL QY by decreasing nonradiative recombination.<sup>23,24</sup> Indeed, if the band gap of the core is enclosed by that of the shell, then the wave functions of electrons and holes are confined within the core region, thus reducing the probability of nonradiative decay into surface states and trap sites.<sup>25,26</sup>

\* To whom correspondence should be addressed. Phone: +33 3 83 17 50 53. E-mail: raphael.schneider@ensic.inpl-nancy.fr.

<sup>†</sup> LCPME, Nancy-University.

<sup>‡</sup> DCPR, Nancy-University.

<sup>§</sup> DPG, Université de Haute Alsace.

<sup>||</sup> IJL, Nancy-University.

<sup>⊥</sup> LIMOS, Nancy-University.

<sup>#</sup> SCMEM, Nancy-University.

Wurtzite ZnO is an important wide band gap semiconductor possessing a band gap energy of 3.37 eV at room temperature and exciton binding energy of 60 meV that has found many applications in electronic and optical devices.<sup>26–28</sup> However, because of the high lattice mismatch between ZnO and CdTe or CdS (29 and 21%, respectively), preparation of core/shell CdTe/ZnO or core/shell/shell CdTe/CdS/ZnO QDs and the effects of the ZnO shell on the optical properties of aqueous CdTe core QDs have not yet been studied. In this work, we report for the first time that the growth of a thin ZnO shell on MPA-stabilized core/shell CdTe/CdS QDs in aqueous solution induces a significant redshift of absorption and emission peaks and an increase in radiative lifetime when the shell layer grew. This evolution is affected by the core size and shell thickness. The structural and photophysical properties of QDs were characterized by transmission electron microscopy (TEM), atomic force microscopy (AFM), X-ray diffraction (XRD), X-ray photoelectron spectroscopy (XPS), dynamic light scattering (DLS), and optical spectroscopy.

## 2. Experimental Procedures

**2.1. Instrument.** All optical measurements were performed at room temperature ( $20 \pm 2$  °C) under ambient conditions. Absorption spectra were recorded on a Perkin-Elmer (Lambda 2, Courtaboeuf, France) UV-visible spectrophotometer. Fluorescence spectra were recorded on a Fluorolog-3 spectrofluorimeter F222 (Jobin Yvon, Longjumeau, France) equipped with a thermostatted cell compartment (25 °C), using a 450 W xenon lamp. The QY values were determined by the equation:  $QY(\text{sample}) = (F_{\text{sample}}/F_{\text{ref}})(A_{\text{ref}}/A_{\text{sample}})(n_{\text{sample}}^2/n_{\text{ref}}^2)QY_{(\text{ref})}$ , where  $F$ ,  $A$ , and  $n$  are the measured fluorescence (area under the emission peak), absorbance at the excitation wavelength, and refractive index of the solvent, respectively. PL spectra were spectrally corrected and quantum yields were determined relative to Rhodamine 6G in ethanol (QY = 94%).<sup>29</sup> Fluorescence lifetimes were measured using the time-correlated single-photon counting technique with FL920-fluorescence lifetime spectrometer (Edinburgh instrument) with the instrument response of  $\sim 1$  ns. The excitation source was an nF900 ns flash lamp. The decays were fitted with the iterative deconvolution method on the basis of the Marquardt–Levenberg algorithm.<sup>30</sup> Such a deconvolution technique<sup>31</sup> allows an overall time resolution down to 0.2 ns. The quality of the exponential fits was checked using the reduced  $\chi^2$  ( $\leq 1.2$ ).

To determine the morphology and diameters of the nanoparticles, the samples were analyzed ex situ by atomic force microscopy (AFM) and transmission electron microscopy (TEM). AFM characterization was carried out using a Digital Instruments Nanoscope III. AFM measurements were done by taping mode using a  $\text{Si}_3\text{N}_4$  tip with resonance frequency and spring constant being 100 kHz and 0.6 N m<sup>-1</sup>, respectively to provide surface topography. TEM and HRTEM images were taken by placing a drop of the particles in water onto a carbon film-supported copper grid. Samples were studied using a Philips CM20 instrument with LaB<sub>6</sub> cathode operating at 200 kV. Dynamic light scattering (DLS) was performed at room temperature using a Malvern zetasizer HsA instrument with an He–Ne laser ( $4 \times 10^{-3}$  W) at a wavelength of 633 nm. The QD aqueous solutions were filtered through Millipore membranes (0.2  $\mu\text{m}$  pore size). The data were analyzed by the CONTIN method to obtain the hydrodynamic diameter ( $d_H$ ) and size distribution in each aqueous dispersion of nanoparticles. XPS measurements were performed at a residual pressure of  $10^{-9}$  mbar, using a KRATOS Axis Ultra electron energy analyzer

operating with an Al K $\alpha$  monochromatic source. Powder (XRD) analyses were obtained using Panalytical X’Pert Pro MPD diffractometer using Cu K $\alpha$  radiation. Crystalline grain sizes were obtained using the size broadening models built into FullProf and an instrumental resolution function obtained with a LaB<sub>6</sub> standard sample.

**2.2. Reagents and Materials.** The chemicals used in the experiments included CdCl<sub>2</sub>, 2.5H<sub>2</sub>O (99%), 3-mercaptopropionic acid (MPA, 99+%), sodium borohydride (96%), tellurium powder (99.9%), Zn(OAc)<sub>2</sub> (99.99%), and iso-propanol (*i*-PrOH, HPLC grade). All chemicals were used without further purification.

**2.3. Preparation of Water-Soluble Core/Shell CdTe/CdS QDs.** The sodium hydrogen telluride NaHTe solution was prepared by reacting NaBH<sub>4</sub> with tellurium powder (2.5/1 molar ratio). Briefly, 37 mg (1 mmol) of sodium borohydride and 50 mg (0.4 mmol) of tellurium powder were added to a small Schlenk flask, and air in the system was pumped off for 30 min and replaced with N<sub>2</sub>. Then, 10 mL of ultrapure water was added. The reaction mixture was heated at 80 °C for 30 min under flowing N<sub>2</sub>. The deep red aqueous solution obtained was immediately used for the preparation of core/shell CdTe/CdS QDs. The concentration of the NaHTe solution was 0.04 M.

The CdTe/CdS QDs were prepared by using the reaction between CdCl<sub>2</sub> and NaHTe in the presence of MPA as the stabilizing agent, following the method described previously<sup>32</sup> with some modifications. The molar ratio of Cd<sup>2+</sup>/Te<sup>2-</sup>/MPA was 2/1/4.8. Briefly, CdCl<sub>2</sub>, 2.5H<sub>2</sub>O, and MPA were dissolved in 100 mL of nitrogen-saturated ultrapure water ([Cd<sup>2+</sup>] = 1.25 or 10.9 mM for reactions performed at 100 °C and at 150 °C, respectively), and the pH was adjusted to 9.0 with 1 M NaOH. Then, the NaHTe solution was added to the above precursor solution. The complex solution with a faint red color was either refluxed at 100 °C for 15 h or put into a Teflon-lined stainless steel autoclave with a volume of 125 mL. The autoclave was maintained at 150 °C for a designed time and then cooled to room temperature. Different-sized CdTe/CdS QDs were prepared by varying the synthesis time (1, 1.5, and 2 h for CdTe/CdS QDs with average diameters of 1.9, 3.1, and 3.4 nm, respectively).

**2.4. Preparation of Core/Shell/Shell CdTe/CdS/ZnO QDs.** The Zn<sup>2+</sup> injection solution (0.01 M) was prepared by dissolving Zn(OAc)<sub>2</sub> in aqueous solution. The molar ratio of Zn/Cd was controlled within 0.2/1 and 1/1. Briefly, the crude CdTe/CdS QDs were first added to a three-necked flask and heated under air at 100 °C. For a Zn/Cd ratio of 0.4/1, 2.5 mL of the Zn(OAc)<sub>2</sub> solution was first injected at a speed of 0.3 mL/min into the solution and further refluxed 1 h. After that period, another 2.5 mL portion of the Zn(OAc)<sub>2</sub> solution was injected, and the mixture was further heated for 1 h. The obtained CdTe/CdS/ZnO QDs were precipitated by adding *i*-PrOH and centrifuged at 4000 rpm. QDs were dried in vacuo at room temperature and redissolved in water. Their concentration was estimated from the reported extinction coefficient per mole of particles ( $\epsilon$ ) by using the Beer–Lambert’s law.<sup>33</sup>

**2.5. Photostability of Core/Shell/Shell CdTe/CdS/ZnO QDs.** The photostability of aqueous dispersions of CdTe/CdS and of CdTe/CdS/ZnO QDs was investigated by irradiating the samples with a 180 mW Hg–Xe lamp under open air condition at room temperature. The distance between the sample solutions and lamp was fixed to 20 cm. Aliquots of the sample solution were taken at regular intervals for PL measurements and absorption characterization.

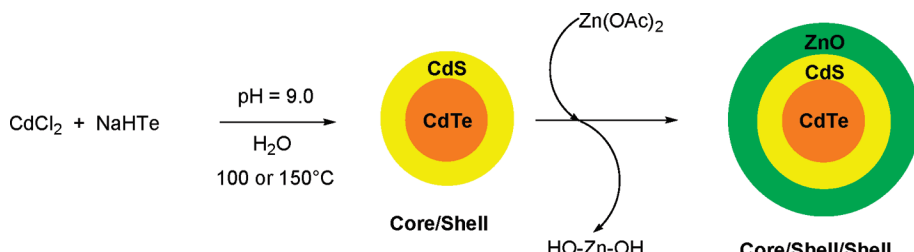


**Figure 1.** Schematic of the synthesis of water-soluble CdTe/CdS/ZnO core/shell/shell QDs.

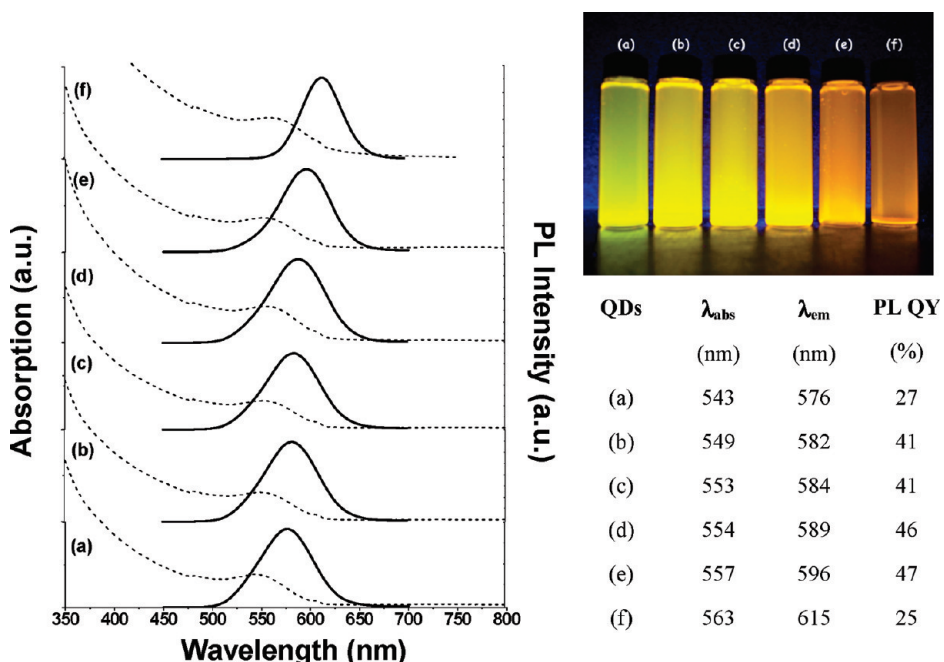


**Figure 2.** Absorption (dotted line) and PL (solid line) spectra after growing the ZnO shell around CdTe/CdS core/shell QDs. (a) CdTe/CdS solution taken at a reflux time of 15 h, (b) Zn/Cd = 0.2, (c) Zn/Cd = 0.4, (d) Zn/Cd = 0.6, (e) Zn/Cd = 0.8, and (f) Zn/Cd = 1.0. Related PL QYs and photograph of the samples under irradiation with 365-nm ultraviolet light from a UV lamp are presented on the right.

### 3. Results and Discussion

Highly luminescent core/shell CdTe/CdS QDs possessing an average diameter of 2.1 nm (determined by TEM) were first prepared in aqueous solution by refluxing CdCl<sub>2</sub> and NaHTe in water for 15 h at pH 9.0 in the presence of MPA.<sup>32</sup> The core/shell/shell QDs were prepared by the slow injection of a 0.01 M aqueous solution of Zn(OAc)<sub>2</sub> to the crude CdTe/CdS QDs and further refluxing for 2 h. At basic pH (pH value measured at the end of the hydrothermal synthesis of CdTe/CdS QDs was found to be 8.7), Zn(OAc)<sub>2</sub> is first hydrolyzed and converted into its hydroxide Zn(OH)<sub>2</sub>. Dehydration of Zn(OH)<sub>2</sub> produces ZnO clusters that grow at the surface of CdTe/CdS nanocrystals to form the ZnO shell (Figure 1).

Zn/Cd molar ratios of 0.2/1, 0.4/1, 0.6/1, 0.8/1, and 1/1 were used to evaluate the influence of the thickness of the ZnO shell on the PL properties of the QDs. Figure 2 displays the representative UV-vis absorption and PL spectra of CdTe core QDs and those of core/shell/shell CdTe/CdS/ZnO QDs after coating the ZnO shell. With the injection of Zn(OAc)<sub>2</sub> solution and further refluxing, the absorbance of CdTe core QDs shifts to longer wavelengths. Typically, after two times adding the Zn<sup>2+</sup> solution to QDs with an average diameter of 2.1 nm and using a Zn/Cd ratio of 0.8, the absorption peak of the resulting core/shell/shell QDs shifted from 543 to 557 nm. Meanwhile, the emission peak shifted from 572 to 596 nm, and the PL QY increased from 27% for the CdTe core QDs to 47% for core/shell/shell CdTe/CdS/ZnO QDs prepared with a Zn/Cd molar

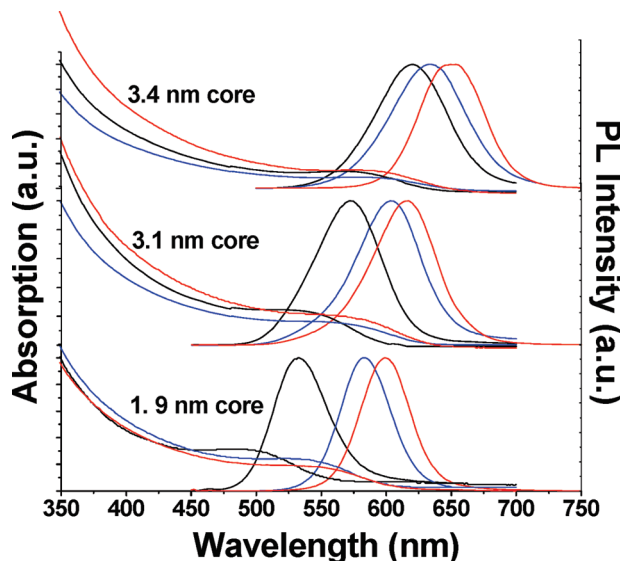
ratio of 0.8/1, revealing a good passivation of the core surface and elimination of surface trap states. The corresponding full width at half-maximum (fwhm) of the emission peaks was maintained during the shell growth, about 60 nm, indicating that relatively monodispersed particles were obtained. Contrary to CdTe QDs covered by a CdS shell,<sup>34</sup> the shape of the first exciton peak remains invariant regardless of the thickness of the ZnO shell. No deep trap luminescence is detected, indicating good emissive properties of the QDs. The good PL QYs of the CdTe/CdS/ZnO QDs can be maintained for several months at ambient temperature. Compared to the corresponding CdTe QDs parent aqueous solution whose PL QY decreased from 27 to 17% after 4 months storage in water at a concentration of 1000 nM, the PL QY of CdTe QDs covered by the ZnO shell (Zn/Cd = 0.8) was virtually identical (46%) after the same storage period. Above a value of 0.8 for the Zn/Cd ratio, a significative drop of the PL QY is clearly measured. Similar observations were ascribed to the strain released through the formation of dislocations in the shell with increasing shell thickness, e.g., for core/shell CdSe/ZnS QDs.<sup>35–37</sup> In our case, the decrease in PL QY was also accompanied by aggregation of QDs indicating a saturation effect. Only very thin shells (<1 monolayer) of the ZnO material can be overcoated on the CdTe/CdS QDs (vide infra), although large excesses of the shell precursor have been used. This situation is probably due to the strong binding capacity of the MPA ligand to the CdTe nanocrystals or CdS shell, which prevents the addition of the shell precursor around

**TABLE 1: Absorption and Emission Wavelengths and PL QYs of CdTe/CdS@MPA QDs before and after ZnO Shell Growth**

material diameter (nm)	CdTe/CdS core			CdTe/CdS/ZnO (Zn/Cd = 0.4)			CdTe/CdS/ZnO (Zn/Cd = 0.8)		
	$\lambda_{\text{abs}}$ (nm)	$\lambda_{\text{em}}$ (nm)	PL QY (%)	$\lambda_{\text{abs}}$ (nm)	$\lambda_{\text{em}}$ (nm)	PL QY (%)	$\lambda_{\text{abs}}$ (nm)	$\lambda_{\text{em}}$ (nm)	PL QY (%)
1.9	486	533	11	526	583	34	541	601	18
3.1	536	572	13	554	603	26	560	617	25
3.4	573	622	53	585	635	56	587	651	47

the core QDs. The use of long-length mercapto alcanoic acid (6-mercaptophexanoic acid, 11-mercaptoundecanoic acid, or dihydrolipoic acid)-stabilized CdTe QDs<sup>17</sup> as core for the growth of the ZnO shell does not have any effects on the absorption and emission. It is likely that the steric bulk of the ligand and/or the formation of a macrocyclic annulus complex that wraps around the CdTe/CdS nanoparticles via the interaction between the carboxyl group of the acid function and surface cadmium atoms completely hinder the formation of the ZnO shell. It is also worth noting that the electrophoretic mobility of CdTe/CdS@MPA QDs on cellulose acetate in a borate buffer (pH 9.0) was not altered by the introduction of the ZnO shell. CdTe/CdS@MPA and CdTe/CdS/ZnO@MPA QDs migrate similarly from the negative pole to positive pole in the electrophoresis run. According to the band gap evolution displayed by the absorption spectra and the gradual increase in PL QY with the thickness of the ZnO shell and invariance of the corresponding emission band widths, we have strong indications that CdTe/CdS/ZnO have typical type-I behavior.<sup>38</sup>

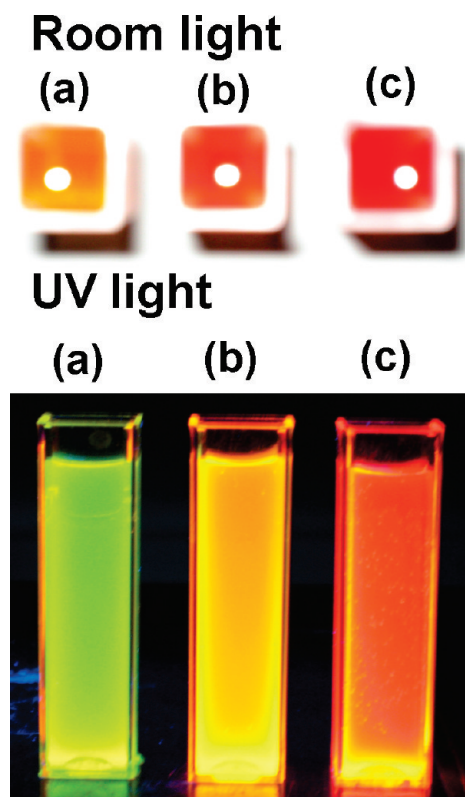
CdTe/CdS@MPA QDs with growing diameters were prepared under hydrothermal conditions at 150 °C by varying the synthesis time and using a Cd<sup>2+</sup>/NaHTe/MPA ratio of 2/1/4.8. Three samples were obtained with average QDs diameters of 1.9, 3.1, and 3.4 nm, and their respective photophysical data are collected in Table 1. The diameter increase in QDs leads to marked redshift of the first exciton peak in absorption and also to a redshift of the fluorescence band whose maximum emission wavelength increases from 533 to 622 nm (Figure 3). When a Zn/Cd ratio of 0.4 is used for the growth of the ZnO shell, absorption and fluorescence bands are strongly red-shifted as compared to that observed for QDs without a ZnO shell. In the meantime, the PL QY is multiplied by a factor 3, 2, and 1.1.



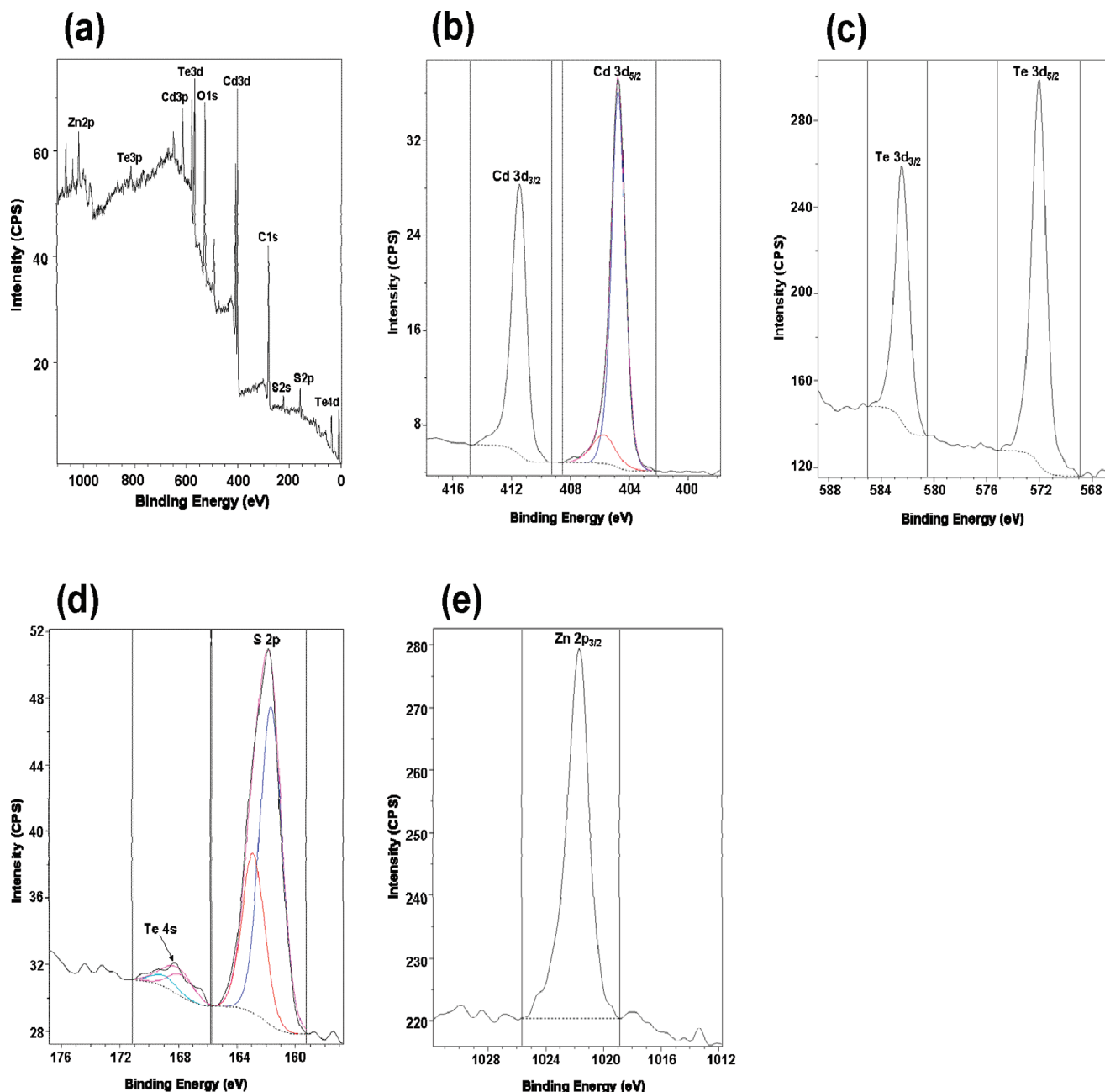
**Figure 3.** Absorption and photoluminescence spectra of CdTe/CdS QDs and of core/shell/shell CdTe/CdS/ZnO QDs after shell growth. Core diameters are given. Two Zn/Cd ratios were used for ZnO shell growth: Zn/Cd = 0.4 (blue line) and Zn/Cd = 0.8 (red line).

Figure 4 shows photographs of the QDs prepared from the CdTe/CdS@MPA core with an average diameter of 3.1 nm. As can be seen, CdTe/CdS/ZnO QDs are very bright, even at normal room light irradiation. It is also worth noting that the magnitude of the redshift is clearly dependent on the core size with a larger spectral shift for smaller QDs. Such an effect was also reported when growing a CdS shell around CdSe QDs.<sup>39</sup>

A low temperature (100 °C) is favorable for good epitaxial growth of the ZnO shell. The aggregation of nanocrystals observed at a Zn/Cd ratio of 1/1 was also obtained when deposition of Zn(OH)<sub>2</sub> was attempted under hydrothermal conditions (120 or 150 °C). Blank experiments also demonstrated that the redshift observed for absorption and emission spectra (Figures 2 and 3) is due to the ZnO shell growth and not to the continuous growth of CdTe QDs or formation of a CdS shell with a larger band gap than that of CdTe<sup>40,41</sup> by basic hydrolysis of the MPA ligand at the surface of CdTe QDs. Moreover, when CdTe/CdS@MPA QDs prepared at 100 °C and isolated from the reaction medium by precipitation with *i*-PrOH were redissolved in water at pH 11.0 and heated for 2 h at 100 °C to force the basic hydrolysis of MPA, a significant redshift was observed in the absorption and PL spectra (about 20 nm starting from green-emitting CdTe@MPA QDs with an average diameter of 1.9 nm,  $\lambda_{\text{abs}} = 486$  nm,  $\lambda_{\text{em}} = 533$  nm, and PL QY



**Figure 4.** Photographs under room light or UV radiation of (a) CdTe/CdS QDs with a diameter of 3.1 nm, (b,c) CdTe/CdS/ZnO QDs prepared from the same core using Zn/Cd ratios of 0.4 and 0.8, respectively.



**Figure 5.** XPS spectra of CdTe/CdS/ZnO QDs. (a) XPS survey spectrum. Binding energy spectra of (b) Cd 3d, (c) Te 3d, (d) S 2p, and (e) Zn 2p.

$= 11\%$ ). This redshift is a direct consequence of the decrease in the kinetic energy of the excited electron and a hole in the nanocrystals because of the spreading of their wave functions into the CdS shell<sup>42</sup> but is much weaker than that obtained after addition of Zn(OAc)<sub>2</sub> (about 50 nm). PL intensity enhancement was also more pronounced after the introduction of the ZnO shell (34%) compared to CdTe/CdS QDs obtained after the forced hydrolysis process (20%). Moreover, upon addition at room temperature of aqueous solutions of Zn(OAc)<sub>2</sub> to a dispersion of 2.3 nm wide CdTe/CdS QDs at pH 9.0 (Zn/Cd ratios were varied from 0.2 to 1.0), the absorption spectra stayed unchanged ( $\lambda_{abs} = 499$  nm). Meanwhile, the fluorescence emissions were gradually redshifted (from 534 to 539 nm) and PL QY increased from 13 to 16.7% (Figure S1 of the Supporting Information). This experiment clearly ruled out the simple coordination of the Zn<sup>2+</sup> cation with negatively charged MPA-capped nanocrystals<sup>43</sup> when the reaction was conducted at 100 °C.

X-ray photoelectron spectroscopy (XPS) is a sensitive tool for the analysis of the chemical composition of materials, and hence, XPS was used to analyze the changes on the surface of MPA-coated CdTe-core QDs by the ZnO shell growth. Figure 5 is the typical XPS spectra of the CdTe/CdS/ZnO nanoparticles, where panel a is the survey spectrum and panels b–e are the high-resolution binding energy spectra for Cd, Te, S, and Zn species, respectively. According to the survey spectrum, the elements Cd, Te, S, Na, O, Zn, and C were detected. The typical peaks of Cd 3d<sub>5/2</sub> at 405.0 eV, Cd 3d<sub>3/2</sub> at 411.6 eV, Te 3d<sub>5/2</sub> at 572.0 eV, Te 3d<sub>3/2</sub> at 582.4 eV, and S 2p at 162.0 eV appeared in all XPS spectra, confirming the existence of cadmium, tellurium, and sulfur in the QDs. During the shell growth, we observed no significant changes for the S 2p<sub>3/2</sub> and S 2p<sub>1/2</sub> doublet at 161.6 and 162.8 eV, respectively, indicating that the coordination situations for S (from the MPA ligand and CdS shell formed during decomposition of MPA) were not affected.<sup>40,44</sup> The peak at around 1021.7 eV comes from Zn 2p<sub>3/2</sub>.

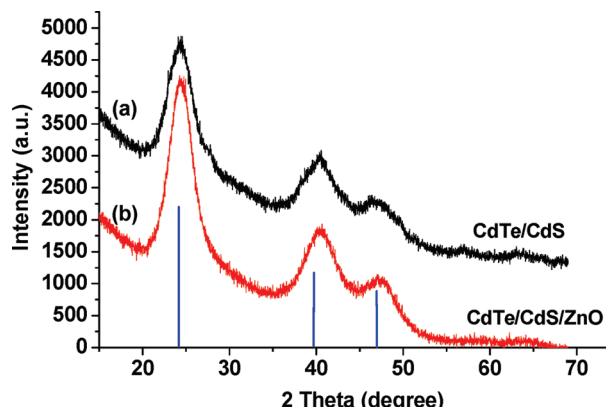


**Figure 6.** XRD patterns of CdTe/CdS@MPA nanocrystals recorded (a) before and (b) after ZnO shell growth. Standard diffraction lines of cubic CdTe are shown at the bottom.

This binding energy is consistent with that of the Zn element linked to oxygen (values between 1021.6 and 1021.9 eV) and confirms that the shell is formed by basic hydrolysis of  $Zn(OAc)_2$  and not by reaction of  $Zn^{2+}$  ions with  $S^{2-}$  ions arising from the decomposition of MPA.<sup>40,44</sup>

Figure 6 displays the X-ray diffraction (XRD) patterns of the starting MPA-stabilized CdTe/CdS cores prepared under hydrothermal conditions possessing an average diameter of 2.1 nm of the core/shell/shell CdTe/CdS/ZnO QDs ( $Zn/Cd = 0.8$ ) precipitated from aqueous solution with an excess of *i*-PrOH, and for comparison, the standard XRD pattern of cubic CdTe is also shown. The broad peaks imply that the nanocrystals are very small. The diffraction pattern of the bare CdTe core QDs is consistent with that of the bulk cubic CdTe structure (JCPDS 75-2086) but slightly displaced toward larger  $2\theta$  values and lies between those inherent to the CdTe and CdS wurtzite phase due to the formation of core/shell CdTe/CdS QDs by decomposition of the MPA ligand at 150 °C. The emergence of the ZnO wurtzite phase was not observed, similar to the formation of a CdS shell on CdTe core QDs reported in the literature.<sup>40,41,45</sup> This could be related to the poor crystallinity of the ZnO layer or to the low content of ZnO in the core/shell/shell nanoparticles. There is no recognizable difference on the positions of XRD reflections between CdTe/CdS@MPA and CdTe/CdS/ZnO@MPA QDs, and XRD patterns have roughly the same shape, which further demonstrates the formation of the core/shell/shell structure and shows that the shell does not disturb the crystalline form of the core. The lattice constant of CdTe nanocrystals at atmospheric pressure is 6.482 Å. The XRD data of the CdTe/CdS QDs prepared and refined with the Rietveld method<sup>46</sup> using the Fullprof program reveal a crystalline structure in a cubic phase *F*43*m* with a reduced lattice constant of 6.398 Å due to the strain imposed by the CdS layer at the surface of CdTe QDs. Because the lattice parameter of wurtzite ZnO ( $a = 3.249$  Å) is considerably smaller than that of CdTe and CdS, the ZnO shell compresses again the CdTe/CdS core. The lattice parameter of CdTe in core/shell/shell QDs is 6.389 Å. Small crystallite sizes manifest in the diffraction pattern by a broadening of the Bragg peaks. Figures S2 and S3 of the Supporting Information show the Rietveld refinements using spherical harmonics for the CdTe system built in the FullProf program.<sup>47</sup> A crystallite size of  $2.0 \pm 1.0$  nm is given with a standard deviation (anisotropy) of 0.23 nm, so we can assume that there is no anisotropic size contribution. This size value correlated well with the results obtained from TEM analysis (vide infra).

Figure 7 shows TEM and HRTEM images of the CdTe/CdS QDs prepared at 100 °C and core/shell/shell CdTe/CdS/ZnO

QDs ( $Zn/Cd = 0.2, 0.4, 0.6, 0.8$ , and 1.0), whose PL spectra are presented in Figure 2. The observed increment in particle size results from the growth of the ZnO shell and correlates well with the  $Zn(OAc)_2$  amount injected in the reaction mixture. This, in turn, proves that the ZnO shell thickness of CdTe/CdS/ZnO QDs can be well-controlled by our synthesis technique. CdTe/CdS@MPA are spherical with an average diameter of  $2.1 \pm 0.5$  nm. Despite the lattice mismatch between CdS and ZnO, core/shell/shell CdTe/CdS/ZnO QDs remain spherical with diameters increasing gradually to 2.2, 2.3, 2.5, and 2.7 nm when varying the  $Zn/Cd$  ratio from 0.2 to 0.8. The diameters estimated from TEM images are coherent with those calculated using the published sizing curve and size-dependent molar extinction coefficient at the first absorption maximum<sup>33</sup> and correlated well with the values obtained from AFM analyses (Figure S4 of the Supporting Information). The average diameter of nanocrystals prepared with a  $Zn/Cd$  ratio of 1/1 increased to 3.1 nm. The strong decrease in PL QY measured for these particles (25%) may either originate from the weaker quantum confinement effect due to the larger particle size or from the strain released through the formation of dislocations in the shell with increasing shell thickness. Because a monolayer of ZnO (distance between consecutive planes along the [002] axis in bulk wurtzite ZnO) is 0.26 nm,<sup>35</sup> the diameter of one monolayer passivated CdTe/CdS QDs would be increased by 0.52 nm. Average diameters of 2.5 and 2.7 nm, respectively, were attained for  $Zn/Cd$  ratios of 0.6 and 0.8 nm (the original core covered by about one monolayer of ZnO) and corresponds to nanocrystals with the highest PL QYs (46 and 47%, respectively).

Aqueous dispersions of native CdTe/CdS QDs and CdTe/CdS/ZnO QDs ( $Zn/Cd = 0.4$ ) were further analyzed by dynamic light scattering (DLS). Figure 8 shows the scattering intensity distributions of both QDs after about 2 days storage in phosphate buffer saline (PBS). The average hydrodynamic sizes determined from DLS data were 13.2 and 9.7 nm, respectively, for MPA-stabilized CdTe/CdS and CdTe/CdS/ZnO QDs, suggesting that the nanoparticles dispersed well in PBS. For both particles, the hydrodynamic diameters were larger than the diameters of the inorganic cores due to the solvation layer around the QDs in the buffer solution. Particle size distribution was also found to be narrower after the growth of the ZnO shell. The two batches of QDs were found to be quite aggregate-free and therefore adequate for biological labeling.

Figure 9 shows the PL decay curves measured at the respective emission peak wavelengths for CdTe/CdS QDs and core/shell/shell CdTe/CdS/ZnO heterostructures ( $Zn/Cd = 0.4$  and 0.8, respectively), whose PL spectra are presented in Figure 2. Nanosecond PL decays of these QDs are shown at the bottom of Figure 9. The decays of all samples are confidently fitted with two exponentials. Such a behavior is often observed for the radiative deactivation of colloidal II–VI QDs.<sup>48–52</sup> The lifetimes  $\tau$  of fast and slow decays are reported in Table 2.

The shorter lifetime can be attributed to exciton recombination,<sup>53,54</sup> while the longer time can be associated with the involvement of surface states in the carrier recombination process.<sup>55–57</sup> It is found that increasing shell thickness results in longer exciton lifetimes. For CdTe/CdS QDs, the average lifetime  $\tau_{av}$  is 17.7 ns. The lifetime lengthens to 28.3 and 33.6 ns for core/shell/shell QDs prepared with  $Zn/Cd$  ratios of 0.4 and 0.8, respectively. The results depicted in Table 2 show that the contribution of nonradiative processes to exciton decay is significantly reduced and/or that exciton trapping at surface defects is less efficient as a consequence of the extra ZnO inorganic shell.

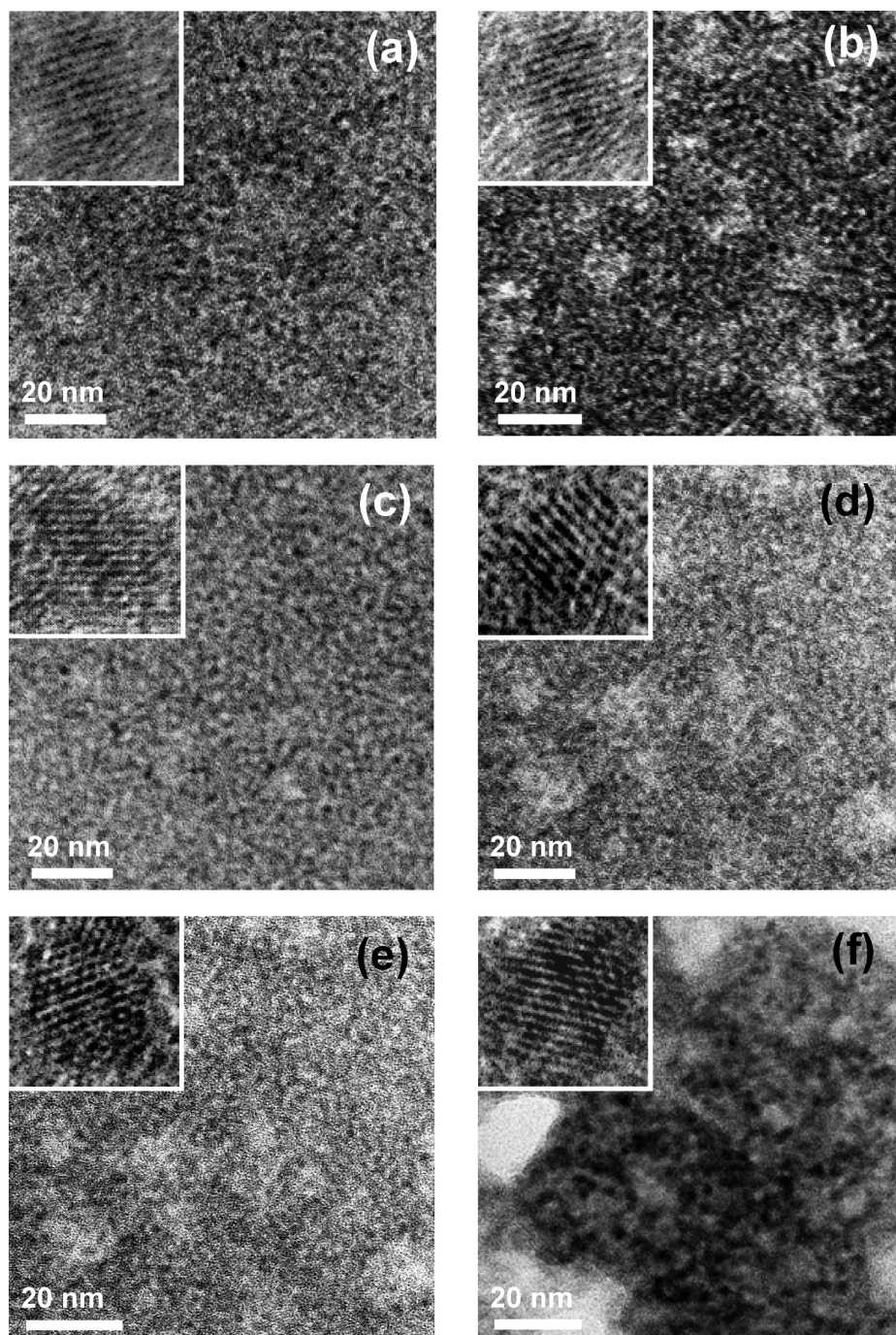


**Figure 7.** TEM and HRTEM (insets) micrographs of (a) CdTe/CdS core QDs and the same core with different thickness shells of ZnO: (b) Zn/Cd = 0.2, (c) Zn/Cd = 0.4, (d) Zn/Cd = 0.6, (e) Zn/Cd = 0.8, (f) Zn/Cd = 1.0.

The QDs have the advantage of long lifetimes under UV or visible excitation over those of organic dyes, and therefore, they can be used as fluorescent labels to examine the long-term kinetics of molecular–cellular interactions. Figure 10 shows the changes in the absorption and fluorescence spectra of MPA-stabilized CdTe/CdS QDs (diameter = 2.3 nm, PL QY = 15%) and of the same QDs covered by a ZnO shell (Zn/Cd = 0.4) in neutral solution during irradiation with a Hg/Xe lamp. Recent studies have shown that photobleaching of thiol-capped QDs was mainly due to oxygen-dependent photooxidation.<sup>58–60</sup> The irradiation of CdTe QDs capped by thioglycolic acid (TGA) promotes oxidation of unsaturated Te atoms, which are known to be highly susceptible to oxidation.<sup>60</sup> Meanwhile, TGA is oxidized and detaches from the QD surface, resulting in

photobleaching and aggregation of QDs. For CdTe/CdS QDs capped with MPA, the initial exciton peak at 500 nm and fluorescence peak at 533 nm exhibited a gradual blueshift to 451 and 521 nm, respectively, during irradiation due to the formation of a CdTe<sub>x</sub>S<sub>1-x</sub> alloyed structure with a larger band gap energy compared to that of pure CdTe QDs.<sup>61–63</sup> Furthermore, it is noted that the bandwidth of the emission increases from 42 to 55 nm. The PL QYs were first enhanced (up to 18.3%) during the first 5 min of the experiment because surface traps were effectively eliminated by photocorrosion and then gradually decreased overtime (7.2% after 10 min irradiation). CdTe/CdS/ZnO QDs showed much smaller shifts in absorption and emission wavelengths, from 542 to 531 nm and from 572 to 563 nm, respectively. As expected, no significant enhance-

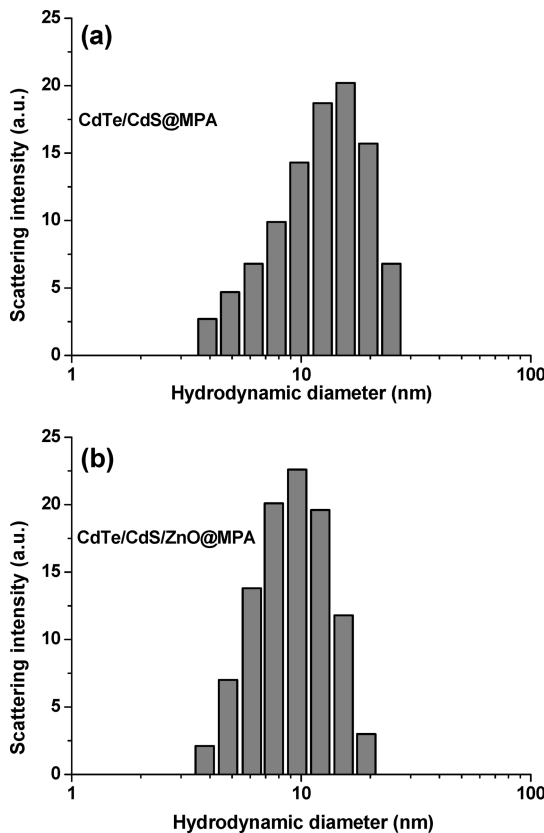


**Figure 8.** Intensity–hydrodynamic size distribution graphs of (a) CdTe/CdS QDs and of (b) CdTe/CdS/ZnO QDs in PBS solution at 25 °C.

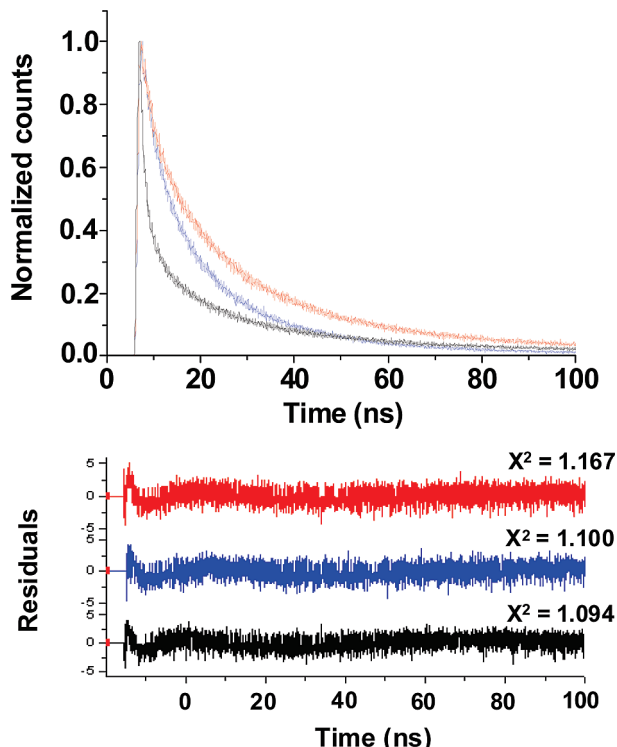


**Figure 9.** Luminescence decay curves of CdTe/CdS (black curve) and CdTe/CdS/ZnO QDs prepared using Zn/Cd ratios of 0.4 (blue curve) and 0.8 (red curve). Excitation wavelength is 405 nm. Lower panel shows weighted residuals for biexponential fits.

ment of the fwhm of PL spectra was observed (from 61 to 62 nm) because of the protection of the ZnO shell. The decrease

**TABLE 2:** Time Constants  $\tau_1$  and  $\tau_2$  and Average Lifetime  $\tau_{av}$  of Core/Shell CdTe/CdS QDs and of Core/Shell/Shell CdTe/CdS/ZnO QDs

sample (ns)	CdTe/CdS	CdTe/CdS/ZnO (Zn/Cd = 0.4)	CdTe/CdS/ZnO (Zn/Cd = 0.8)
$\tau_1$	23.8	36.6	46.0
$\tau_2$	7.4	10.9	11.5
$\tau_{av}$	17.7	28.3	33.6

in PL QYs was constant (from 27 to 21%) after 10 min irradiation but less marked than with CdTe/CdS QDs, thus demonstrating that the ZnO shell enhances the photostability of CdTe/CdS/ZnO QDs.

The usefulness of the engineered nanoparticles for bioimaging applications was investigated using a staining test of surface-attached microbial communities (biofilms) using green- or red-emitting CdTe/CdS/ZnO QDs. Biofilms of *Shewanella oneidensis* were grown for 48 h under the constant flow (200  $\mu$ L/min) of a LML medium<sup>64</sup> supplemented with fumarate (0.5 mM) in flow cell systems that can be accommodated on a microscope setup. After the growth period, a 250 nM solution of QDs was injected via a syringe pump, and incubation was performed for 5 min. Unbound QDs were removed by washing the biofilm with a fresh culture medium. Comparison of the phase contrast image (Figure 11a) and of the Z-scan image (Figure 11b) shows that QDs were quite homogeneously distributed in the biofilm. Higher magnification confocal images (data not shown) demonstrate that CdTe/CdS/ZnO@MPA QDs only associate with some *S. oneidensis* cells, while their accumulation in extracellular polymers or association with proteins was more marked. Figure 11c shows that the typical mushroom structure of the biofilm can readily be identified through fluorescence imaging with CdTe/CdS/ZnO QDs. Finally, it should be noted that the MPA-stabilized QDs are not degraded during the experiment time when interacting with the biofilm as the different QDs used retained their distinct wavelength-specific emission properties.

The dependence of QD photobleaching on the irradiation time of the confocal microscope was also studied. The focused beam of the 405 nm diode of the confocal microscope was fixed at the selected spot (about 1  $\mu$ m in diameter using a 100x objective lens) and 500 nM aqueous dispersions of CdTe/CdS or CdTe/CdS/ZnO (Zn/Cd = 0.4) QDs were submitted to constant irradiation with measuring PL intensity every 10 s. Under low power intensity (about  $0.14 \times 10^{-3}$  W), both QDs were found to be stable. When the power intensity was increased to  $1.2 \times 10^{-3}$  W, both QDs were bleached over the experiment time (Figure 12) but PL decrease in core/shell/shell CdTe/CdS/ZnO QDs was slower and exhibited a half-lifetime three times longer as that of QDs without the ZnO shell. This clearly demonstrates that the presence of ZnO improves the QDs photostability.

## Conclusions

In this study, a simple, cheap, and versatile synthesis of water-soluble core/shell/shell CdTe/CdS/ZnO QDs stabilized by 3-mercaptopropionic acid possessing high photoluminescence quantum yields was developed under the moderate temperature of hydrothermal growth. Depending on the Zn/Cd ratio used and diameter of the CdTe/CdS core, we found the emission color could be tuned in a large spectral range from green to red. After growth of the ZnO shell, the room-temperature fluorescence quantum yields reached values up to 50–60% for orange-red emitting samples, and luminescence lifetimes were increased. The ease of processing and good PL properties in aqueous solution of the core/shell/shell CdTe/CdS/ZnO QDs prepared

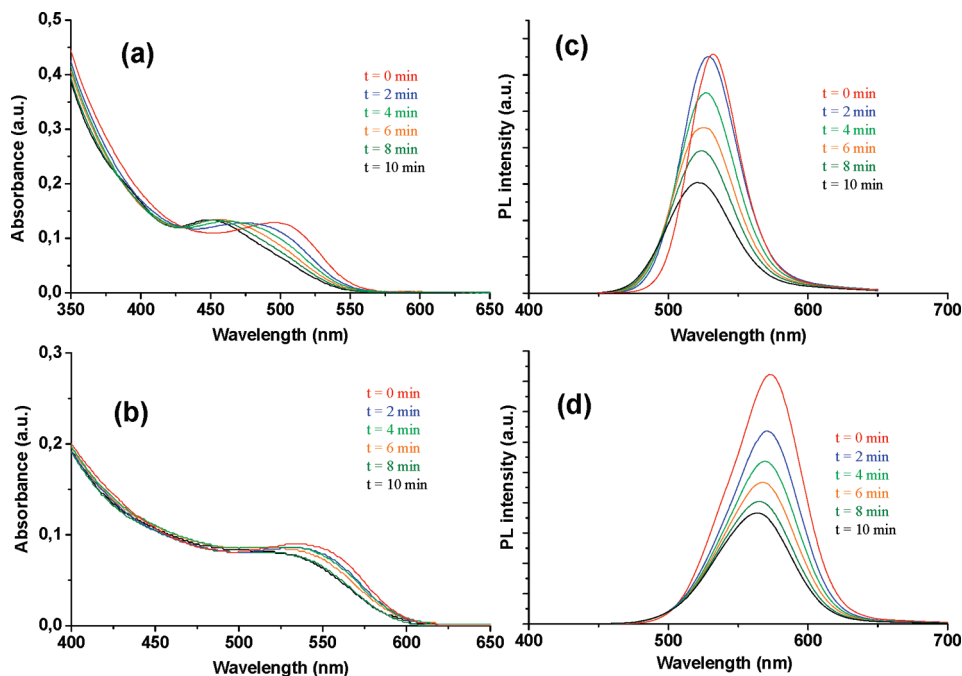


**Figure 10.** Time evolutions of absorption and PL spectra of (a,c) CdTe/CdS QDs and (b,d) CdTe/CdS/ZnO QDs under irradiation of a Hg/Xe lamp.

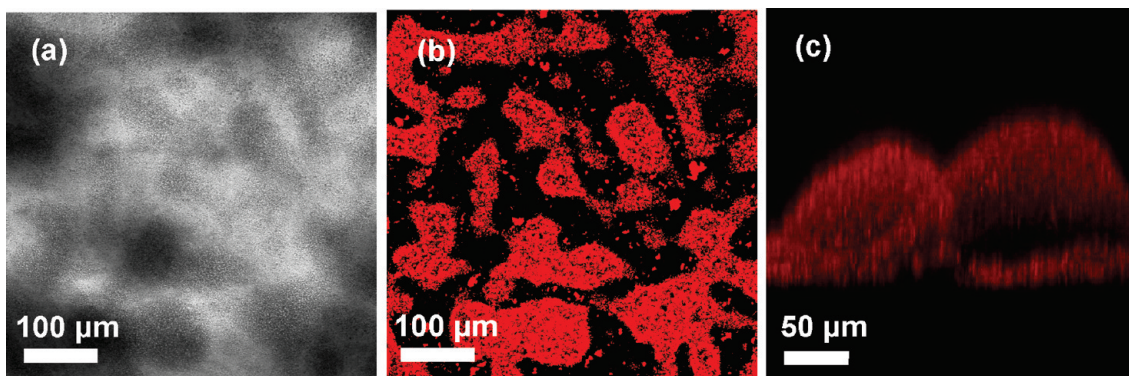


**Figure 11.** Confocal microscopy images of a *S. oneidensis* biofilm treated with CdTe/CdS/ZnO@MPA QDs: (a) transmission image, (b) corresponding XY plane fluorescence image, and (c) sum of XY planes. Confocal microscopy images were obtained with laser excitation at 405 nm.

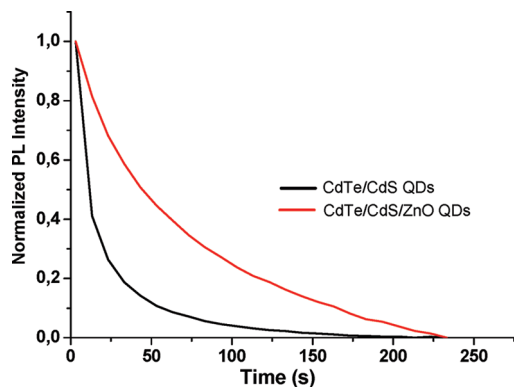


**Figure 12.** Photobleaching of CdTe/CdS and CdTe/CdS/ZnO QDs under the focused beam of a confocal diode (405 nm,  $1.2 \times 10^{-3}$  W) as a function of time.

have great potential in biolabeling and lasing applications of semiconductor nanocrystals.

**Acknowledgment.** This work was supported by the Agence nationale pour la Recherche (ANR blanc 07, project DYNA-BIO). We express our gratitude to Dr. Jacques Lambert

(LCPME, Nancy-University) and Olivier Soppera (DPG, Mulhouse), respectively, for acquiring the XPS spectra and AFM images. The authors thank Dr. Serge Corbel (DCPR-Nancy University) for facilitating photostability experiments. The authors also thank Dr. Christophe Merlin (LCPME, Nancy-University) for helpful discussions and Dr. Marie-José Stebe (SRSMC, Nancy-University) for DLS measurements.

**Supporting Information Available:** Evolution of absorbance and emission spectra of CdTe/CdS QDs upon addition of Zn(OAc)<sub>2</sub> at room temperature, AFM characterization of CdTe/CdS and CdTe/CdS/ZnO QDs, and Rietveld refinement results of the powder XRD data of core/shell CdTe/CdS and of core/shell/shell CdTe/CdS/ZnO QDs. This material is available free of charge via the Internet at <http://pubs.acs.org>.

## References and Notes

- Bruchez, M. P.; Moronne, M.; Gin, P.; Weiss, S.; Alivisatos, A. P. *Science* **1998**, 281, 2013.
- Chan, W. C. W.; Nie, S. M. *Science* **1998**, 281, 2016.
- Medintz, I. L.; Uyeda, H. T.; Goldman, E. R.; Mattoussi, H. *Nat. Mater.* **2005**, 4, 435.
- Weng, J.; Ren, J. *Curr. Med. Chem.* **2006**, 13, 897.

- (5) Sun, Q. J.; Wang, Y. A.; Li, L. S.; Wang, D. Y.; Zhu, T.; Xu, J.; Yang, C. H.; Li, Y. F. *Nat. Photonics* **2007**, *1*, 717.
- (6) Han, M.; Gao, X.; Su, J. Z.; Nie, S. *Nat. Biotechnol.* **2001**, *19*, 631.
- (7) Alivisatos, A. P. *Nat. Biotechnol.* **2004**, *22*, 198.
- (8) Rosi, N. L.; Mirkin, C. A. *Chem. Rev.* **2005**, *105*, 1547.
- (9) Michalet, X.; Pinaud, F. F.; Bentolila, L. A.; Tsay, J. M.; Doose, S.; Li, J. J.; Sundaresan, G.; Wu, A. M.; Gambhir, S. S.; Weiss, S. *Science* **2005**, *307*, 538.
- (10) Qu, L.; Peng, X. G. *J. Am. Chem. Soc.* **2002**, *124*, 2049.
- (11) Talapin, D. V.; Mekis, I.; Gotzinger, S.; Kornowski, A.; Benson, O.; Weller, H. *J. Phys. Chem. B* **2004**, *108*, 18826.
- (12) Blackman, B.; Battaglia, D.; Peng, X. *Chem. Mater.* **2008**, *20*, 4847.
- (13) Wuister, S. F.; Swart, I.; Driel, F. V.; Hickey, S. G.; Donega, C. M. *Nano Lett.* **2003**, *3*, 503.
- (14) Rogach, A. L.; Kornowski, A.; Gao, M.; Eychmüller, A.; Weller, H. *J. Phys. Chem. B* **1999**, *103*, 3065.
- (15) Nikoobakht, B.; Burda, C.; Braun, M.; Hun, M.; El-Sayed, M. A. *Photochem. Photobiol.* **2002**, *75*, 591.
- (16) Zhong, P.; Yu, Y.; Wu, J.; Lai, Y.; Chen, B.; Long, Z.; Liang, C. *Talanta* **2006**, *70*, 902.
- (17) Aldeek, F.; Balan, L.; Lambert, J.; Schneider, R. *Nanotechnology* **2008**, *19*, 475401.
- (18) Zhang, Y.; Gao, S.; Ying, J. Y. *Adv. Mater.* **2007**, *19*, 376.
- (19) Mao, W.; Guo, J.; Yang, W.; Wang, C.; He, J.; Chen, J. *Nanotechnology* **2007**, *18*, 485611.
- (20) Zheng, Y.; Yang, Z.; Ying, J. Y. *Adv. Mater.* **2007**, *19*, 1475.
- (21) He, Y.; Sai, L.-M.; Lu, H. T.; Hu, M.; Lai, W.-Y.; Fan, Q.-L.; Wang, L.-H.; Huang, W. *Chem. Mater.* **2007**, *19*, 359.
- (22) Alivisatos, A. P. *J. Phys. Chem.* **1996**, *100*, 13226.
- (23) Balet, L. P.; Ivanov, S. A.; Piryatinski, A.; Achermann, M.; Klimov, V. *Nano Lett.* **2004**, *4*, 1485.
- (24) Yang, H.; Holloway, P. H. *Adv. Func. Mater.* **2004**, *14*, 152.
- (25) Mokari, T.; Banin, U. *Chem. Mater.* **2003**, *15*, 3955.
- (26) Meulenkamp, E. A. *J. Phys. Chem. B* **1998**, *102*, 5566.
- (27) Fu, Y.-S.; Du, X.-W.; Kulinich, S. A.; Qiu, J.-S.; Qin, W.-J.; Li, R.; Sun, J.; Liu, J. *J. Am. Chem. Soc.* **2007**, *129*, 16029.
- (28) Houskova, V.; Stengl, V.; Bakardjeva, S.; Murafa, N.; Kalendova, A.; Oplustil, F. *J. Phys. Chem. A* **2007**, *111*, 4215.
- (29) Fischer, M.; Georges, J. *Chem. Phys. Lett.* **1996**, *260*, 115.
- (30) Connor, D. V.; Phillips, D. *Time Correlated Single Photon Counting*. Academic Press: London, 1984.
- (31) Ven, M. V. D.; Ameloot, M.; Valeur, B.; Boens, N. *J. Fluoresc.* **2005**, *15*, 377.
- (32) Li, L.; Qian, H.; Fang, N.; Ren, J. *J. Lumin.* **2006**, *116*, 59.
- (33) Yu, W. W.; Qu, L. H.; Guo, W. Z.; Peng, X. G. *Chem. Mater.* **2003**, *15*, 2854.
- (34) Zeng, Q.; Kong, X.; Sun, Y.; Zhang, Y.; Tu, L.; Zhao, J.; Zhang, H. *J. Phys. Chem. C* **2008**, *112*, 8587.
- (35) Dabboussi, B. O.; Rodriguez-Viejo, J.; Mikulec, F. V.; Heine, J. R.; Mattoossi, H.; Ober, R.; Jensen, K. F.; Bawendi, M. G. *J. Phys. Chem. B* **1997**, *101*, 9463.
- (36) Talapin, D. V.; Mekis, I.; Gotzinger, S.; Kornowski, A.; Benson, O.; Weller, H. *J. Phys. Chem. B* **2004**, *108*, 18826.
- (37) Xia, R. G.; Kolb, U.; Li, J. X.; Basché, T.; Mews, A. *J. Am. Chem. Soc.* **2005**, *127*, 7480.
- (38) Li, J. J.; Wang, Y. A.; Guo, W. Z.; Keay, J. C.; Mishima, T. D.; Johnson, M. B.; Peng, X. G. *J. Am. Chem. Soc.* **2003**, *125*, 12567.
- (39) Mekis, A.; Talapin, D. V.; Kornowski, A.; Haase, M.; Weller, H. *J. Phys. Chem. B* **2003**, *107*, 7454.
- (40) Bao, H.; Gong, Y.; Li, Z.; Gao, M. *Chem. Mater.* **2004**, *16*, 3853.
- (41) He, Y.; Lu, H.-T.; Sai, L.-M.; Lai, W.-Y.; Fan, Q.-L.; Wang, L.-H.; Huang, W. *J. Phys. Chem. B* **2006**, *110*, 13370.
- (42) Peng, X.; Schlamp, M.; Kadavanich, A. V.; Alivisatos, A. P. *J. Am. Chem. Soc.* **1997**, *119*, 7019.
- (43) Susha, A. S.; Munoz Javier, A.; Parak, W. J.; Rogach, A. L. *Colloids Surf., A* **2006**, *281*, 40.
- (44) Meissner, D.; Benndorf, C.; Memming, R. *Appl. Surf. Sci.* **1987**, *27*, 243.
- (45) Wang, C. L.; Zhang, H.; Zhang, J. H.; Li, M. J.; Sun, H. Z.; Yang, B. *J. Phys. Chem. C* **2007**, *111*, 2465.
- (46) Rietveld, H. M. *J. Appl. Crystallogr.* **1969**, *2*, 65.
- (47) Rodríguez-Carvajal, J. *Recent Developments of the Program FullProf*. Commission on Powder Diffraction Newsletter 26; International Union of Crystallography (IUCr): Ottawa, December 2001.
- (48) Kapitonov, A. M.; Stupak, A. P.; Gaponenko, S. V.; Petrov, E. P.; Rogach, A. L.; Eychmueller, A. *J. Phys. Chem. B* **1999**, *103*, 10109.
- (49) Wang, X.; Qu, L.; Zhang, J.; Peng, X.; Xiao, M. *NanoLett.* **2003**, *3*, 1103.
- (50) Franzl, T.; Koktysh, D. S.; Klar, T. A.; Rogach, A. L.; Feldmann, J. *Appl. Phys. Lett.* **2004**, *84*, 2904.
- (51) Wuister, S. F.; van Driel, F.; Meijerink, A. *Phys. Chem. Chem. Phys.* **2003**, *203*, 1253.
- (52) Petrov, E. P.; Cichos, F.; Zenkevich, E.; Starukhin, D.; von Borczyskowski, C. *Chem. Phys. Lett.* **2005**, *402*, 233.
- (53) Klimov, V. I.; Mc Branch, D. W.; Leatherdale, C. A.; Bawendi, M. G. *Phys. Rev. B: Condens. Mater.* **1999**, *60*, 13740.
- (54) Zhang, J. Y.; Wang, X.-Y.; Xiao, M. *Opt. Lett.* **2002**, *27*, 1253.
- (55) Bawendi, M. G.; Carroll, P. J.; Wilson, W.; Brus, L. *J. Chem. Phys.* **1992**, *96*, 946.
- (56) Efros, A. L.; Rosen, M.; Kuno, M.; Nirmal, M.; Norris, D. J.; Bawendi, M. G. *Phys. Rev. B* **1996**, *54*, 4843.
- (57) Wang, X. Y.; Qu, L.; Zhang, J. Y.; Peng, X. G.; Xiao, M. *Nano Lett.* **2003**, *3*, 1103.
- (58) Samia, A. C. S.; Chen, X.; Burda, C. *J. Am. Chem. Soc.* **2003**, *125*, 15736.
- (59) Zhang, Y.; He, J.; Wang, P.-N.; Chen, J.-Y.; Lu, Z.-J.; Lu, D.-R.; Guo, J.; Wang, C.-C.; Yang, W. L. *J. Am. Chem. Soc.* **2006**, *128*, 13396.
- (60) Ma, J.; Chen, J.-Y.; Zhang, Y.; Wang, P.-N.; Guo, J.; Yang, W.-L.; Wang, C.-C. *J. Phys. Chem. B* **2007**, *111*, 12012.
- (61) Resch, U.; Weller, H.; Henglein, A. *Langmuir* **1989**, *5*, 1015.
- (62) Mekis, I.; Talapin, D. V.; Kornowski, A.; Haase, M.; Weller, H. *J. Phys. Chem. B* **2003**, *107*, 7454.
- (63) Steckel, J. S.; Snee, P.; Coe-Sullivan, S.; Zimmer, J. P.; Halpert, J. E.; Anikeeva, P.; Kim, L.-A.; Bulovic, V.; Bawendi, M. G. *Angew. Chem., Int. Ed* **2006**, *45*, 5796.
- (64) Teal, T. K.; Lies, D. P.; Wold, B. J.; Newman, D. K. *Appl. Environ. Microbiol.* **2006**, *72*, 7324.